CHAPTER 10

Micro- and Nano-Fabrication of Biodegradable Polymers

S. C. Chen and Y. Lu
Department of Mechanical Engineering, The University of Texas at Austin, Austin, Texas 78712 USA

CONTENTS

1. INTRODUCTION

Recent advances in micro- and nano-fabrication technologies have enhanced the tools available to create clinically important therapeutic applications. A variety of implantable and oral drug delivery devices based on silicon, glass, silicone elastomers, or plastic materials have been successfully developed [1–5]. Such devices would permanently remain in biological tissues if not removed surgically. Because of the inherent difficulty in retrieving small-scale devices from tissues, it is advantageous to use biodegradable polymers that would naturally degrade and disappear in tissue over a desired period of time. Biodegradable polymer conduits and tissue engineering scaffolds have been produced using extrusion, fiber bonding, salt

ISBN: 1-58883-053-5/$00.00

Handbook of Biodegradable Polymeric Materials and Their Applications
Edited by Surya Mallapragada and Balaji Narasimhan
Volume 1: Pages (1–17)

Table 1. List of some biodegradable polymers for biomedical applications.

Polymer	T_m(°C)	T_g(°C)	Tensile Modulus (MPa)	Degradation Time (months)
Polyglycolic acid	225 ~ 230	35 ~ 40	7	6 ~ 12
L-Polylactic acid	173 ~ 178	60 ~ 65	2.7	>24
DL-Polylactic acid	Amorphous	55 ~ 60	1.9	12 ~ 16
Polycaprolactone	58 ~ 63	(−65) ~ (−60)	0.4	>24
85/15 poly(DL-lactide-co-glycolide)	Amorphous	50 ~ 55	2.0	5 ~ 6

leaching, and laminating [6–8]. However, micro- and nano-fabrication of biodegradable polymers with precise control over surface microarchitecture, topography, and size remains an important challenge. Traditionally, silicon-based microelectromechanical systems (MEMS) are fabricated by the repeated application of unit processing steps such as thin film deposition, photolithography, and etching. Unfortunately, these methods are not suitable for biodegradable polymers. In recent years, significant efforts have been devoted to developing novel micro- and nano-fabrication techniques for biodegradable polymers.

Over the past decade, the use of biodegradable polymers for the administration of pharmaceuticals and biomedical devices has increased dramatically. The most important biomedical applications of biodegradable polymers are in the areas of controlled drug delivery systems [9], and in the forms of implants and devices for bone and dental repairs [10, 11]. Biodegradable polymers can be either natural or synthetic. In general, synthetic polymers offer greater advantages over natural ones in that they can be tailored to give a wider range of properties [12]. The general criteria for selecting a polymer for use as a degradable biomaterial are to match the mechanical properties and the degradation rate to the needs of the application. Commonly used biodegradable polymers, along with their selected physical and chemical characteristics, are listed in Table 1. Poly(D-lactic acid) (PDLA) is a biodegradable polymer with extensive medical applications due to its biodegradable property, which has been proven harmless to human body cells. PDLA has been used as a substrate material for potential applications in nerve regeneration in the field of tissue engineering. Poly(ε-caprolactone) (PCL), an aliphatic polyester, is one of the most important biodegradable polymers in medicine. Some of the applications of PCL are sutures and biocompatible medical devices. Poly(vinyl alcohol) (PVA) is used in a wide range of applications such as adhesives, fibers, textile, paper sizing, and water-soluble packaging. It is also used to modify the degradation profile of other polymers [13, 14, 15]. These polymers have unique features such as controllability of mechanical properties, ability to tailor degradation rates, and minimal toxicity and immune response that make them ideal for medical uses. In the following sections, we will present several micro- and nano-fabrication techniques developed for biodegradable polymers.

2. LASER MICROMACHINING

The development of lasers has been an exciting chapter in the history of science and engineering because they have significant potential for applications in many scientific and engineering fields. As a light source, a laser beam offers several unique features for materials processing. Monochromaticity is one of the unique characteristics of laser light. Perfectly monochromatic light cannot be produced (even by a laser), but laser light is many times more monochromatic than the light from any other sources. Since the absorption coefficient of different materials is highly wavelength-dependent, by selecting the laser wavelength from deep ultra-violet (DUV) to infrared (IR), one can precisely control the manner of material processing. Moreover, the processing depth can be controlled because the optical penetration depth, L_{op} depends on the wavelength, according to $L_{op} = \lambda/4\pi k$, where λ is the wavelength and k is the extinction coefficient of the solid material [16].

Coherent light waves all travel in the same direction (spatial coherence) at the same frequency and in phase (temporal coherence). This gives rise to a very narrow beam and

the intense, pure light that characterizes a laser. The spatial coherence allows one to focus the beam very tightly. For a high-powered laser, this results in a very high energy density for laser ablation and thin film deposition or material redistribution [17]. The ability to focus the laser beam down to a micron level provides the means for precise laser processing in extremely small dimensions. This is fully utilized in bioengineering applications to minimize the damage to surrounding tissues [18]. For a low power probing laser, tighter focusing makes it possible to achieve "point detection" in surface diagnostics, providing a fine spatial resolution [19].

The variety of laser pulse widths, ranging from continuous wave (CW) to millisecond (10^{-3} seconds), nanosecond (10^{-9} seconds), picosecond (10^{-12} seconds) and even femtosecond (10^{-15} seconds), enables laser applications for various purposes. A CW laser beam can be used for the continuous detection of transient phenomena of materials processing. Nanosecond lasers have been used for precision surface texturing and tissue cutting [20, 21]. Picosecond and femtosecond lasers offer unique advantages for the removal of a precise amount of materials with minimum thermal damage to the surrounding materials. Such short laser pulses also make it possible to process dielectric materials such as glass, due to avalanche ionization and multiphoton effects [22].

Moreover, the laser materials interaction process is noninvasive. Its noncontact nature eliminates possible contamination from processing tools and measurement error due to the contacting sensing elements. It also enables the remote control and monitoring of manufacturing process [23].

2.1. Lasers for Micropatterning

Laser micromachining makes it possible to pattern polymeric materials on the microscale. Photons of the laser light act as "clean particles," and the laser irradiation is essentially noninvasive and is a single-step process. The most popular lasers used for machining polymers are the UV lasers, including excimer, argon-ion, tripled and quadrupled Nd : YAG, fluorine, helium-cadmium, metal vapor, and nitrogen lasers [24]. The small wavelengths allow strong interactions of the beam with a variety of materials. If the incident photon energy is high enough to break the chemical bonds of the target material directly, the material is dissociated into its chemical components and no liquid phase transition occurs. This photochemical process has greatly minimized heat effects compared to the photothermal process involved in visible and infrared lasers. This important feature makes UV laser micromachining very attractive for biodegradable polymer materials, since thermal damage to the nonmachined part can be minimized. Alternative tools for micromachining polymers are femtosecond solid-state lasers with a near-infrared (NIR) wavelength, ultra-short pulse, and high peak power. In polymers, the extremely high laser intensities generated with femtosecond pulses can produce very high concentrations of free electrons via multiphoton absorption and avalanche ionization. Such strongly nonlinear interaction processes can further enhance the localization of the excitation energy, thus increasing the resolution in surface patterning [25].

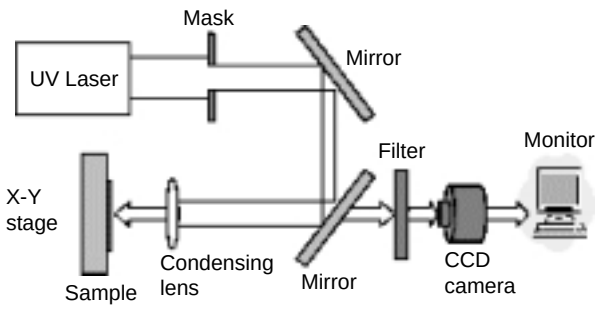

Figure 1. Schematic setup of a laser micromachining system.

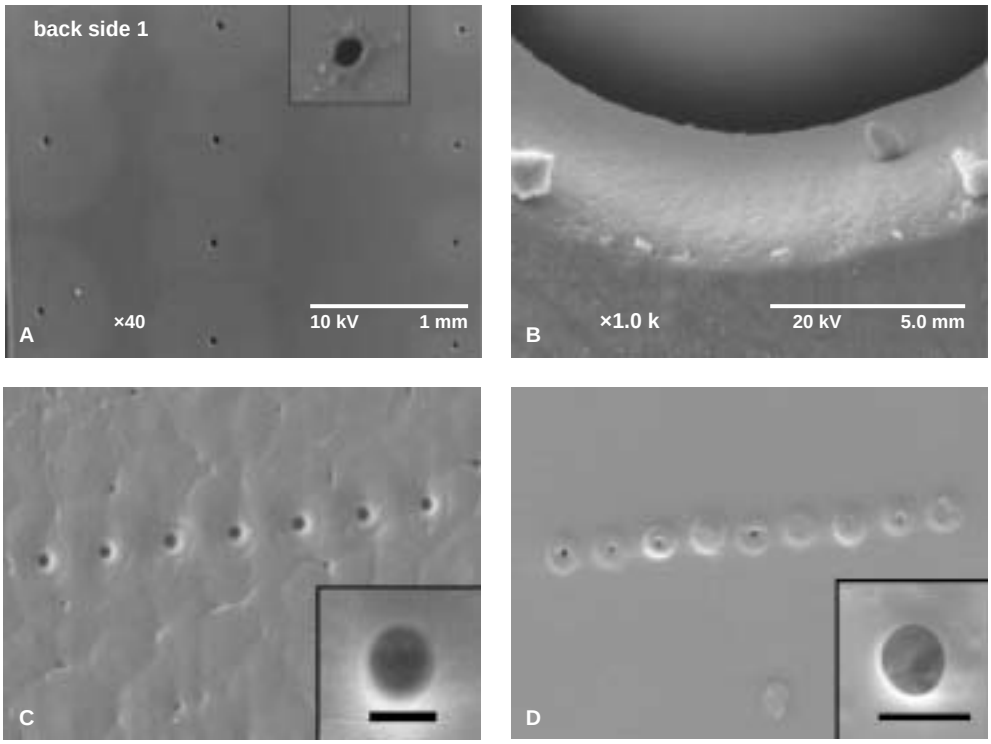

Figure 2. Laser-drilled microholes in (a) PVA by a 266-nm laser; (b) PVA by a 193-nm laser; (c) PCL by a 700-nm femtosecond laser (10 μm in diameter); (d) PDLA by a 700-nm femtosecond laser (8 μm in diameter).

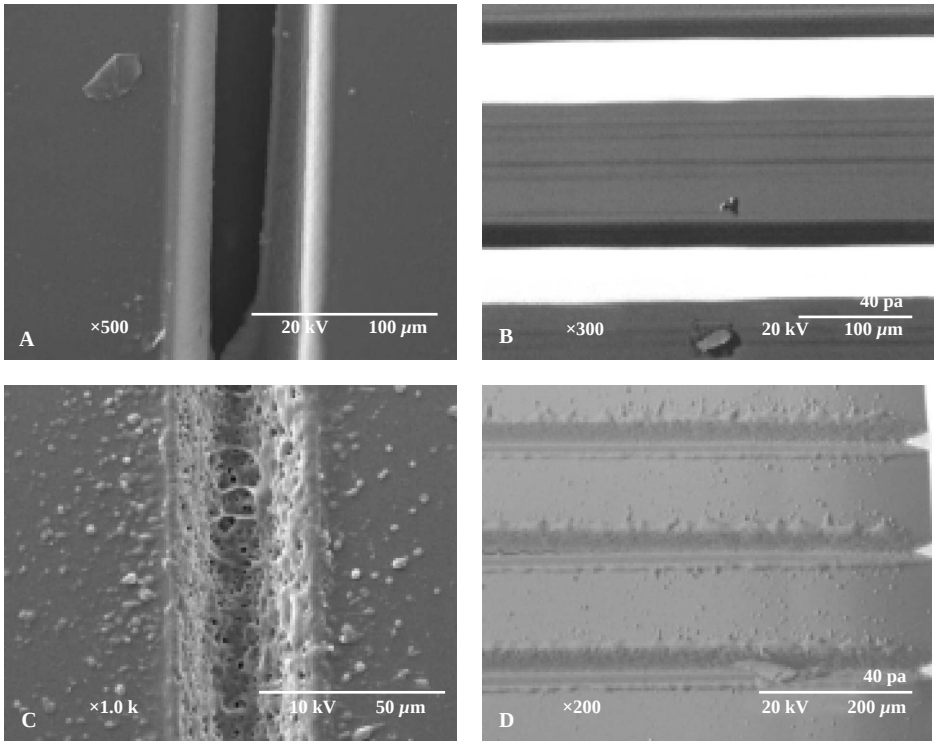

Figure 3. Laser-ablated microchannels in (a) PVA by a 193-nm laser; (b) PDLA by a 193-nm laser; (c) PVA by a 308-nm laser; (d) PDLA by a 308-nm laser.

Table 2. Properties of lasers used in this study.

Lasers	ArF	Nd : YAG	XeCl	Ti:Sapphire
Wavelength (nm)	193	266	308	700
Pulse energy (mJ)	5	275	300	0.007
Repetition rate (Hz)	$10 \sim 100$	$1 \sim 10$	$1 \sim 100$	15, 000
Pulse width (ns)	6	$6 \sim 7$	20	0.15

2.2. Laser Micropatterning of Polymers

We have used a variety of lasers to pattern biodegradable polymers [26, 27]. The micromachining setup for biodegradable polymer ablation consists of four main parts: a laser system, a beam delivery system, a micrometer-resolution x-y sample stage, and an online monitoring system (Fig. 1). The beam delivery system consists of a mask, field lens, turning mirrors, and an imaging lens for micromachining. A spherical lens was used to drill microholes, while a cylindrical lens was used to produce micron-sized channel-type patterns. A charge-coupled device (CCD) camera coupled with a television monitor is used to provide online machining information.

A frequency-quadrupled Nd : YAG laser at 266 nm and a solid-state femtosecond laser at 700 nm (with a Gaussian beam profile) were used to fabricate microhole arrays (Fig. 2). A circular mask was used to shape the beam. A XeCl excimer laser (308 nm) and an ArF excimer laser (193 nm with a uniform beam profile) were used to irradiate the polymers to fabricate microchannels (Fig. 3). Lenses with 25-mm and 50-mm focal lengths were used to obtain microchannels with different groove widths. The arrays of holes drilled could be used as degradable microfilters or drug reservoirs, while the channels could be used for microfluidic delivery systems. All the experiments were conducted in ambient air. Details of the lasers used in this work are listed in Table 2.

No melting or redeposition was noticed in the case of 193-nm laser [Fig. 2(b), Fig. 3(a,b)], but resolidified polymer debris was found around the machined holes and channels at wavelengths of 308 nm and 266 nm [Fig. 2(a), Fig. 3(c,d)]. This is because at the 308-nm wavelength, the photon energy of light is only 4.02 eV. This energy is not high enough to break the polymer bonds. At the 193-nm wavelength, the photon energy of the laser beam reaches about 7.9 eV, which is well above the bond energies of the polymer. The femtosecond laser delivered a clean cut on the edges of the holes [Fig. 2(c,d)]. The irregularities in the hole shape can be attributed to the spherical aberration and noncircularity of the original laser beam. By using advanced beam delivery systems and beam shapers, the irregularity of the hole shape can be corrected.

Another potential feature of laser ablation is the capability of surface modification of microfabricated structures concurrent with structure formation (e.g., channels) [28]. Many reactive species are formed both at the polymer surface and in the gas phase during the laser ablation process. Reaction of these ablation products at the nascent channel walls can result in surface chemical functionality that is significantly different from that in the bulk of the polymer [29]. For example, incorporation of nitrogen or oxygen can give rise to amino, hydroxyl, carboxylic, or phenolic functional groups at the surface [30]. These types of surface functionalities are thought to play an important role in electro-osmotic flow, a commonly used means to pump solution through microchannels [31].

3. NANOSPHERE LITHOGRAPHY

Laser direct patterning provides a resolution on the order of microns due to the optical diffraction limit of the laser wavelength, which is $\lambda/2\text{NA}$, where λ is the wavelength and NA is the numerical aperture of the focusing lens. A typical value of NA in air is from 0.5–1.0. Therefore, the machining resolution is on the order of λ. In order to achieve nanoscale resolution, near-field photolithographic techniques were developed for nanostructuring by delivering a laser beam through a hollow near-field tip or illuminating the tip of a scanning probe microscope with a pulsed laser [32, 33]. A strong local optical field was established

between the sample surface and the sharp tip when the surface/tip gap was of a few nanometers (Fig. 4). Structures with lateral dimensions below 30 nm and, therefore, well below the minimal resolvable feature size of half the wavelength of the light, were produced underneath the tip [34, 35, 36]. However, this type of near-field nanolithographic technique has hardly been used in an industrial setting due to its limited throughput, hollow tip blockage, and difficulty in process control.

We used a new approach involving the illumination of a monolayer of a nanometer-sized sphere array using a laser beam to pattern a solid surface in a mass production fashion (Fig. 5) [37, 38, 39]. A spherical particle may act as a lens and, therefore, intensifies the incoming laser beam if the sphere diameter is larger than the laser wavelength. Near-field enhancement may play an important role if the diameter of the spherical particle is equal or smaller than the wavelength.

3.1. Sample Preparation and Processing

Probably the first report in which ordered monolayers of colloidal particles were systematically utilized for the fabrication of submicroscopic surface structures was published in 1981 [40]. A suspension of colloidal particles with a diameter of 312 nm was applied onto a glass plate and allowed to evaporate. Afterward, a small portion of the glass plate was covered with a monolayer of hexagonally arranged spheres. The experiments carried out by Denkov and coworkers [41] revealed for the first time the mechanism of the self-assembly process that eventually leads to hexagonally close-packed arrays of colloidal particles. Array formation proceeds in two steps: First, a nucleus is formed when the thickness of the solvent layer (generally water) approaches the diameter of the particles. When the top of the particles protrudes from the water surface, it is deformed and, due to surface tension effects, the spheres are pulled together. Theoretical calculations have shown that these lateral capillary forces can exceed the thermal energy (k_BT) of the particles by many orders of magnitude [42]. In the second step, evaporation of the solvent from the micromenisci between the spheres causes water influx from outside, which is related to convective particle transport toward the nucleus. The aforementioned method is simple but results in a poorly organized monolayer. Since the quality of the resulting patterns strongly depends on the properties of the substrate as well as on how homogeneous the process of evaporation is, we focused our efforts on obtaining an efficient treatment to clean the substrate and, at the same time, we controlled the temperature and the humidity of the system by means of common tools.

PCL thin films with a flat surface (surface roughness in the order of 10 nm) were prepared and used as a substrate for better investigation, even though a flat surface is not required for this process. A simple chamber consists of a hot-plate, and a rubber lid was used to control the temperature and humidity. As shown in Figure 6, the sample substrate was placed on the hot-plate and covered by the rubber lid. The setup was tilted about 10 degrees. The rubber lid provided a relatively good thermal stability as well as protected the surface from the external air flow.

A 1% (wt/vol) colloid of silica spheres (diameter = 640 nm) was dropped onto the PCL substrate. In this way, the evaporation starts from the top of the sample on a horizontal

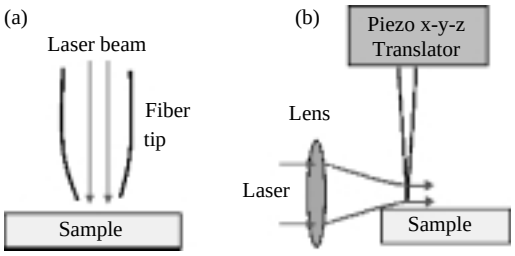

Figure 4. Schematics of near-field nanofabrication techniques by (a) delivering a laser beam through a hollow near-field tip or (b) illuminating the tip of a scanning probe microscope with a pulsed laser. A strong local optical field was established between the sample surface and the sharp tip when the surface/tip gap was of a few nanometers.

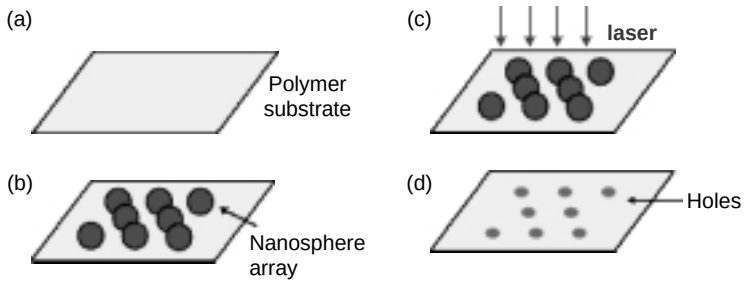

Figure 5. Schematic illustration of procedures for nanosphere lithography. (a) A polymer substrate. (b) Monolayer of nanosphere array is deposited. (c) Laser irradiation. (d) Holes are generated on the substrate.

border where evaporation takes place. This border then moves to the bottom of the sample until it is completely dry. The speed of evaporation and the quality of the resulting sample depends on this angle; 10 degrees was used on all samples presented here. The deposition on the silicon substrate covered about 1 cm^2, but only a small portion of the area was covered by hexagonally close-packed monolayers [Fig. 7(a)], which included a variety of defects that arise as a result of nanosphere polydispersity, site randomness, point defects, and line defects. The rest of area was the part where the evaporation took place last, at the bottom of the sample. We believe that in such regions the remaining water concentrated impurities and the excess particles, creating multilayers and clusters.

With a setup similar to that of laser micromachining, samples were irradiated with the second and third harmonic wave of a Nd : YAG laser or an ArF excimer laser. The laser beam was focused by a lens (f = 50.8 mm) onto the sample mounted on a three-dimensional precision stage. All experiments were performed under ambient conditions.

3.2. Nanostructure Formation

Most of the spheres in the round shape area that were exposed to the laser pulse with the diameter of 10 μm disappeared, leaving holes with the same hexagonal pattern as the spheres were formed on the PCL surface [Fig. 7(b)]. A similar phenomenon was observed in Fig. 9(c), where spheres at the monolayer edge and adjacent holes were aligned in a hexagonal arrangement and, therefore, the spheres located themselves on the holes.

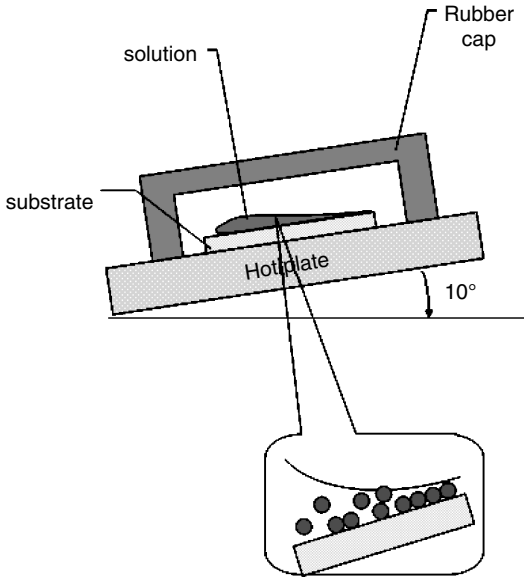

Figure 6. A simple chamber consists of a hot-plate and a rubber lid. It was used to control the temperature and humidity. The spheres start to form a close-packed monolayer on the edge of the water meniscus.

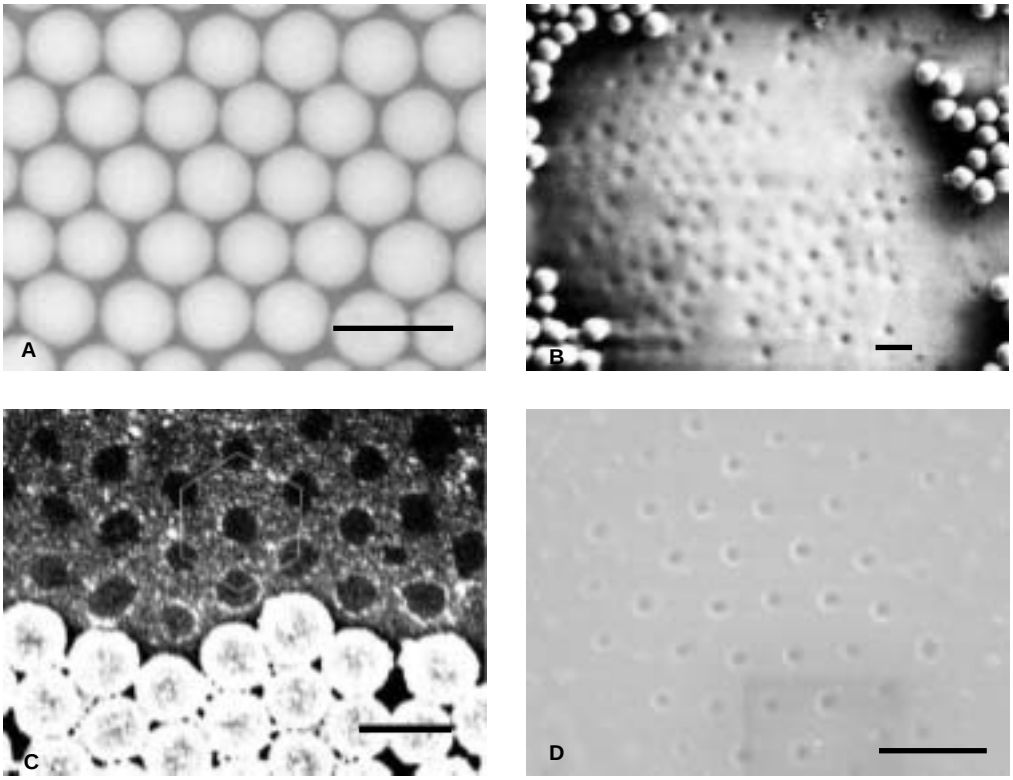

Figure 7. (a) Self-assembled nanosphere monolayer in close-packed hexagonal form. (b) Nanohole array in PCL by 355-nm laser. Spheres at the monolayer edge and adjacent holes are aligned in a hexagonal arrangement. (c) Nanohole array in PCL by 266-nm laser. (d) Nanohole array in PCL by 193-nm laser.

Laser energy was varied from a minimum threshold energy, below which no clear nanostructure was observed, to a maximum energy, beyond which the polymer surface was ablated directly by the laser pulse. In three cases, the diameter of the hole was 430 nm [Fig. 7(c)], 360 nm [Fig. 7(b)], and 240 nm [Fig. 7(c)], corresponding to 355 nm, 266 nm, and 193 nm laser wavelengths, respectively, and remained unchanged within the experiment laser energy range. As the laser wavelength decreases, the features are cleaner. The enhanced optical field by nanospheres in the near-field region, which, we believe, produces nanoscale features, can be explained by Mie scattering. When the diameter of the sphere is equal or greater than the wavelength, light is scattered elastically according to the Mie Scattering Law. The electric field around a Mie sphere (sphere diameter larger than the laser wavelength) is enhanced by several times that of the incident light toward the forward area of the sphere [43, 44].

One advantage of this process lies in its simplicity and massively parallel capability for nanoscale surface patterning. Future work is needed on characterizing changes in surface chemical properties in laser-processed areas.

4. REPLICATION TECHNIQUES

Replication technologies have proven useful for biodegradable polymer microfabrication because the principles behind these processes are straightforward and well known in the macroworld. The underlying principle is the replication of a microfabricated mold tool, which represents the inverse geometry of the desired polymer structure. The expensive microfabrication step is only necessary for the initial fabrication of this master structure, which can can be replicated many times into the polymer substrate. In addition to the cost advantage, replication techniques also offer the benefit of the freedom of design—the master can be fabricated with a large number of different microfabrication technologies, which allow various geometries to be realized.

4.1. Microimprinting Lithography

Microimprinting lithography, also known as "hot embossing" or "compression molding," is one of the most widely used processes to fabricate microstructures for data storage, wave gratings, or microfluidic applications [13, 45–47]. In these reports on hot embossing, a master with a microscale relief structure on the surface was first fabricated by standard MEMS techniques. A thin layer of chromium was coated on a quartz wafer by evaporation coating. A layer of electron beam resist (a polymer that is sensitive to electron beams; PMMA is often used.) was then spun-cast on the chromium layer. In an electron beam lithographic machine, the electron beam resist was selectively exposed to the focused electron beam. Exposed resist was dissolved in the developer, leaving the electron beam resist layer with desired patterns. The wafer was exposed to the chromium etchant, which took away the chromium that was not covered by the electron beam resist. Thus, a pattern was transferred to the chromium layer. The quartz substrate was etched using reactive ion etching (RIE) through the chromium mask, leaving areas covered by chrome. After removing the chrome, the quartz substrate was silanized by exposure to the vapor of $CF_3(CF_2)_6(CH_2)_2SiCl_3$ for approximately 30 minutes. We used this mold as a microdie to transfer the geometric micropatterns from the mold to the biodegradable polymer. The process is illustrated in Figure 8.

PCL films were obtained by casting a PCL chloroform solution (80% wt/vol) onto a glass wafer. They were then placed on the quartz die and heated between two plates just below the melting temperature T_m, which is 57°C. A vacuum was applied to prevent the formation of air bubbles due to entrapped air. A 500-psi (3.4-MPa) pressure was placed between two plates for 10 minutes. The temperature was lowered gradually to release internal stress from the crystallization and different thermal expansion coefficients of the master and the polymer film. The resulting PCL film with a surface pattern was easily peeled off. The geometry was inversed to the one of the quartz mold, while the corners were rounded and the walls were slightly distorted (Fig. 9). Adhesion between the mold and the polymer was minimized by the carbon fluoride surface coating. The pattern distortion was due to the remaining internal stress built up at the corners and to the lack of robustness of the material itself. This fast, relatively inexpensive technique is capable of patterning nanoscale features on a planar surface. However, it requires the thermoplastic polymer to have good thermal stability near the glass transition temperature (T_g).

4.2. Soft Lithography

Soft lithography is a general term of several nonphotolithographic techniques based on self-assembly and replica molding for micro- and nano-fabrication. In soft lithography,

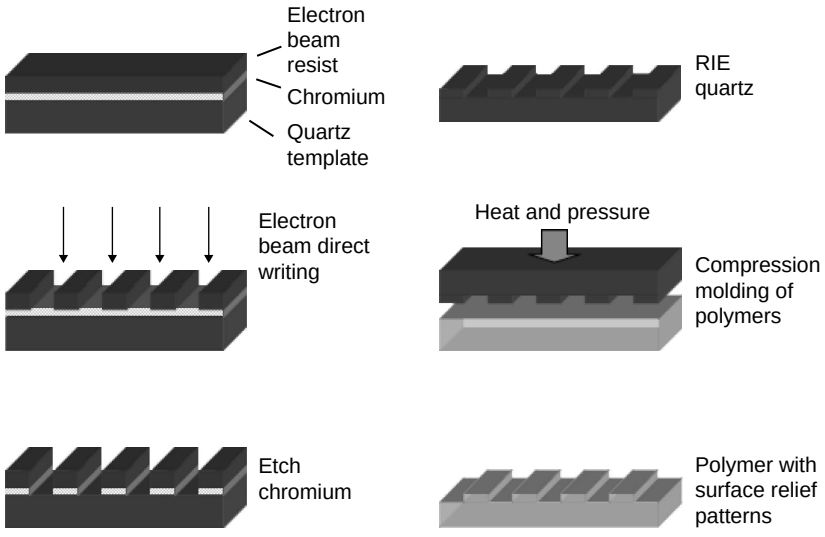

Figure 8. Schematic illustration of procedures for hot embossing.

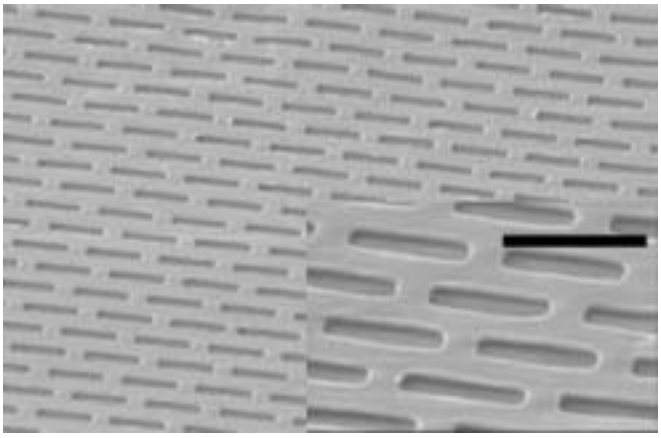

Figure 9. Hot embossed microfeature in PCL. Scale bars in 5 μm.

an elastomeric stamp with patterned relief structures on its surface is used to generate patterns and structures with feature sizes ranging from 30–100 μm. This convenient, effective, and low-cost method has been widely used in micro- and nanofabrication, particularly in fabrication of various biomedical micro- and nanodevices [48, 49]. Xia et al. have provided a detailed review of soft lithographic techniques [50].

The essential element of this technique is the elastomeric stamp prepared by cast molding a crosslinkable elastomer over a master with surface relief structures. As shown in Figure 10, a quartz master was fabricated using e-beam lithography and RIE, as introduced in the previous section. Alternatively, a master can also be produced using standard photolithographic processes on an SU-8 photoresist. A thin layer of SU-8 photoresist was spun-cast on a silicon wafer. This layer was then selectively exposed to UV light via a photomask. (A photomask is usually a quartz plate coated with chromium layer that has desired patterns. The UV light is blocked in the chromium-covered area, while the rest of the areas are transparent.) A surface relief structure was formed after the unexposed photoresist was washed away. In this case, the thickness of the SU-8 layer is critical since it determines the height of the structure on the replica. A poly(dimethylsiloxane) (PDMS) elastomer (Sylgard™ 184) kit, including a liquid silicone rubber base and a curing agent, was mixed and poured over the quartz master.

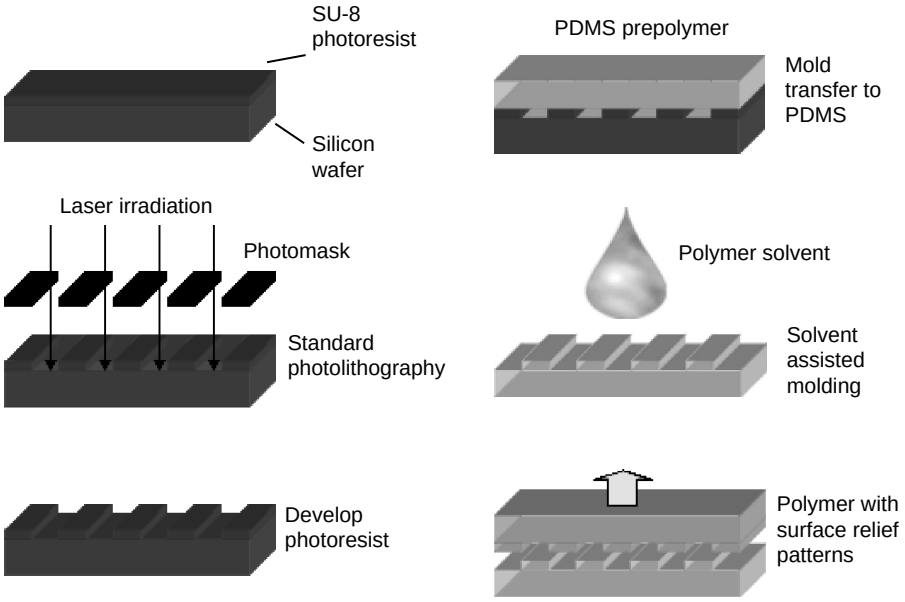

Figure 10. Schematic illustration of procedures for solvent-assisted molding.

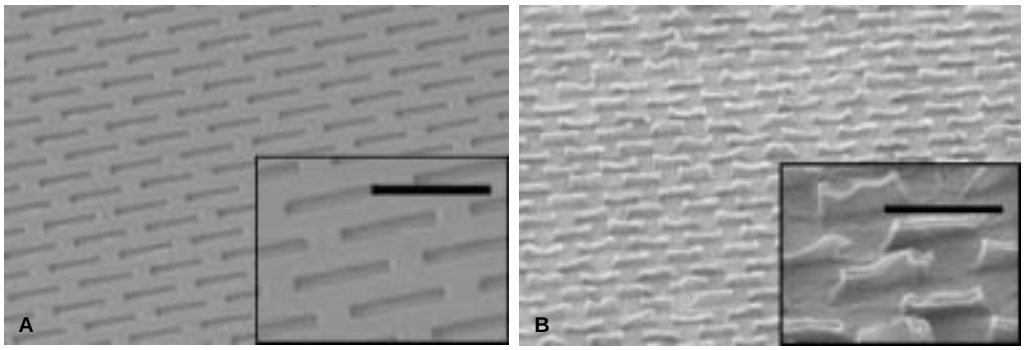

Figure 11. (a) PDMS stamp made by replica molding; (b) PCL film with surface relief structures fabricated by solvent-assisted molding. Scale bars in 5 μm.

The liquid was heated and solidified at 70°C within a few hours via hydrosilylation reaction. The PDMS stamp was ready to use after it was peeled off [Fig. 11(a)].

We used solvent-assisted molding as a demonstration of soft lithographic techniques. A drop of PCL solution in chloroform (80% wt/vol) was placed on a glass wafer. The PDMS stamp was then applied with low force to the liquid against the wafer. The solvent was evaporated at room temperature for 24 hours before the PCL film formed and was peeled off from the stamp. The PCL film had a surface relief structure conformal to the structure on the quartz master, despite imperfections caused by adhesion between PCL and the PDMS stamp [Fig. 11(b)].

5. RAPID PROTOTYPING TECHNIQUES

Rapid prototyping techniques have been applied to manufacturing components with complex geometries beyond the reach of conventional precision machining. The fabrication process is directed by computer-aid design (CAD) of a certain component. Methods including direct deposition [51, 52, 53], selective laser sintering [54], three-dimensional printing [55], and stereolithography [56, 57, 58] have been developed recently, which build components in a laminated fashion.

5.1. Direct Deposition Methods

Direct deposition microfabrication techniques, which are essentially microscale extrusion, were solely derived from their macrofabrication counterpart [51]. A pressure-assisted microsyringe method was used to create a poly(lactic-co-glycolic) acid (PLGA) scaffold with microscale porosity [52]. The system, illustrated in Figure 12, consists of a stainless steel

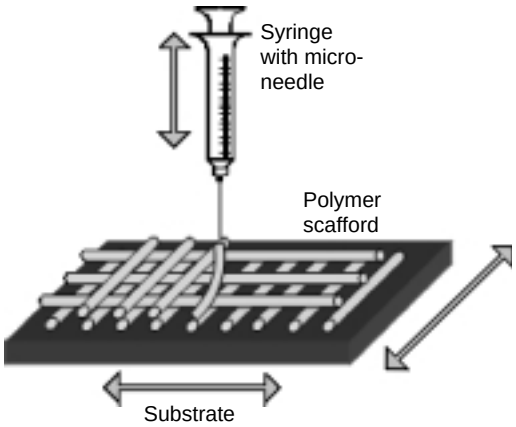

Figure 12. Schematic setup of a pressure-assisted microsyringe method.

syringe with a 10–20-mm glass capillary needle. A solution of the polymer in a volatile solvent is placed inside the syringe and expelled from the tip by the application of filtered compressed air. The syringe is mounted on the z-axis of a three-axis micropositioning system that has a resolution of 0.1 mm. A supporting substrate, usually glass, is placed on the x-y horizontal stage that moves relative to the syringe. The lateral dimension of the structures deposited is between 5–600 mm, depending on the pressure applied to the syringe, the viscosity of the solution, the motor speed, and the dimensions of the syringe tip. The entire system, including valves, pressure regulators, sensors and position controllers, is interfaced with a computerized controlling system that allows a wide range of patterns with a well-defined geometry to be designed and deposited. After the first layer has been deposited, subsequent layers are deposited by moving the syringe up along the z-axis by an amount corresponding to the height of each layer. In theory, each layer can consist of a different polymer or pattern, thus allowing a wide range of three-dimensional structures to be fabricated.

Similarly, PCL scaffolds were fabricated using the micro-extrusion of PCL filaments under several MPa, resulting in a resolution of several hundred microns [53]. Three-dimensional scaffolds can be made by stacking two-dimensional layers in both techniques.

These direct deposition methods are automated and have dynamic control of the scaffold. Although they are essentially serial processes, the throughput is reasonably good for many purposes, requiring relatively simple and inexpensive facilities. However, only limited geometries can be fabricated by these deposition methods, since the upper layer must be supported by the lower one(s). Moreover, only a few polymers are suitable for these methods because the polymer solutions must be highly viscous and the solvents must be volatile. Some solvents are undesirable in terms of potential health risk and the need for regulatory approval.

5.2. Three-Dimensional Printing

Three-dimensional printing has demonstrated the capability of fabricating microstructures and controlling local composition with a high resolution in the interior of the component [55]. From a computer model (CAD) of the desired part, a slicing algorithm draws detailed information for every layer. Each layer begins with a thin distribution of powder spread over the surface of a powder bed. Using a technology similar to ink-jet printing, a binder material selectively joins particles where the object is to be formed. A piston that supports the powder bed and the part-in-progress lowers so that the next powder layer can be spread and selectively joined. This layer-by-layer process repeats until the part is completed (Fig. 13). Unbound powder is removed, leaving the fabricated part. The local microstructure within the component can be controlled either by changing the binder that is printed or by changing the printing parameters during the component construction.

Devices consisting of PCL and polyethylene oxides (PEOs) were fabricated to demonstrate control of drug delivery profiles by controlling the position, composition, and microstructure [55]. The top and bottom layers of the device were constructed by binding PCL power

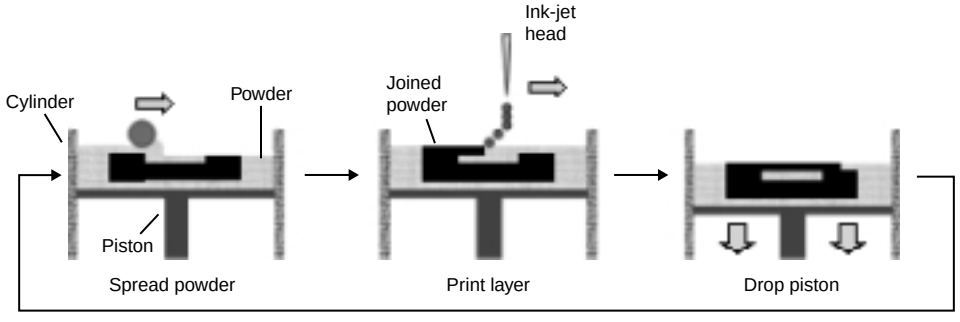

Figure 13. Schematic operation of three-dimensional printing.

into thin solid layers. A cellular-type pattern was printed with PEO, which has a faster degradation rate, in the intermediate layers. Dyes, which represent drugs, were selectively and manually placed within the cells.

The fabrication sequence is described as follows. First, a bead of PCL powder is spread into a thin layer on the piston. Droplets of 20% acid-modified PCL LPS-60HP (PCL-LPS)/chloroform binder solution are deposited on the PCL powder layer through a 45-μm orifice plate to form a solid PCL sheet. PCL particles bind to each other according to the pattern of the printhead motion as the binder contacts the PCL layer. Lines of PCL are formed by moving the printhead in a linear motion. A dense PCL sheet is formed by repeatedly printing lines directly adjacent to each other. The piston is then lowered and ready for the next layer of powder. The second layer begins by spreading PEO powders on the top of the solid PCL sheet. A square grid pattern of five cells by five cells can be made by printing six parallel lines at 3-mm interline spacing, and then repeating another set of six lines at 90 degrees to the first set by rotating the piston. Twenty-five cells, which serve as drug reservoirs, are formed by 20 layers of PEO grid pattern. Different dyes are selectively dropped into the unbound PEO powder before a top layer of dense PCL sheet is printed to seal the cells. Different release mechanisms can be achieved with this technique by controlling device wall composition, anisotropy, and microstructure [55].

5.3. Laser Stereolithography

Laser stereolithography is a method that allows real three-dimensional microfabrication in a manner similar to three-dimensional printing but working in a liquid environment [56, 57, 58]. A three-dimensional solid model designed with CAD software is numerically sliced into a series of two-dimensional layers with an equal thickness [59]. The code generated from each sliced two-dimensional file is then executed to control a motorized x-y-z platform immersed in a liquid photopolymer. The liquid polymer is selectively exposed to a focused laser light, which moves in x-y directions. The polymer cures and becomes solid at the focal point only. After the first layer is formed, the platform moves downward and a new layer of polymer is solidified according to the design (Fig. 14). This layer-by-layer micromanufacturing enables complex internal features, such as complex passageways and curved surfaces, to be accurately produced. Furthermore, by using different proteins and microparticles containing polymer solutions for each layer (or even for partial layers), we are able to create a precise spatial distribution of biochemical microenvironments.

PLGA (50:50) microparticles encapsulating fluorescein or rhodamine isothiocyanate were used as a model drug containing microparticles [59]. Polyethylene glycol dimethacrylate (PEGDMA, M_w 1,000) was mixed with a cytocompatible photoinitiator (Darocure 2959) along with different microparticles. This mixture was photopolymerized, layer-by-layer, using a frequency-tripled Nd : YAG laser (355 nm) and a micromanipulator stage. Different spatial distributions of the microparticles were created and evaluated using a laser scanning

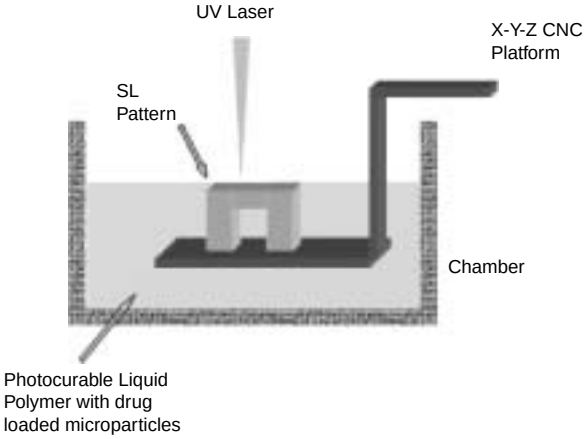

Figure 14. Schematic setup of a laser stereolithography system.

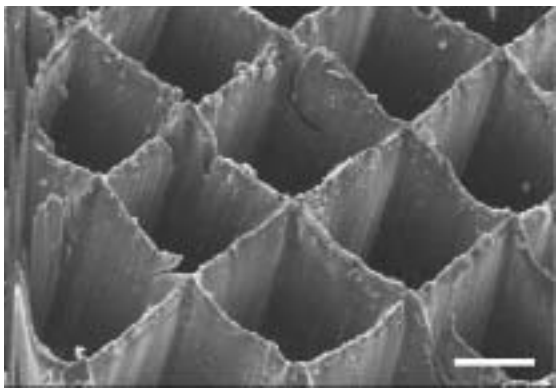

Figure 15. Cellular-type structure produced by laser stereolithography. Fluorescein microparticles were embedded in PEG-DMA walls. 400 × 400-μm pore size.

confocal microscope to optimize the laser energy, initiator concentration, accuracy of spatial distribution, et cetera.

A cellular structure is shown in Figure 15. Square pores were formed by solidifying vertical walls with a 400-μm interline spacing. We can also control the spatial distribution of fluorescein and rhodamine microparticles inside a photocrosslinked polymer layer. A cellular structure containing fluorescein microparticles (1 μm in diameter) and a quadrant structure, with precisely controlled distribution of fluorescein and rhodamine microparticles (5 μm in diameter), are shown in Figure 15(a) and (b). A computer-reconstructed cross section of a particle contained two-layer structure is shown in Figure 15(c). As indicated, precise, predesigned distributions of controlled release biofactors could be engineered within such scaffold structures [59].

Among all the factors that affect the quality of the products, the photocurable polymer resin is the most sensitive to stereolithography. Because the products are used for biomedical scaffold purposes, the requirements of the resin are as follows:

1. Biocompatible, and in some cases, biodegradable
2. Low viscosity
3. Stable under visible light
4. Fast curing speed
5. Compatible with three-dimensional polymerization
6. Reasonably good accuracy and mechanical strength

PEGDMA was chosen here because it is biocompatible. This hydrogel polymer has been used in a variety of *in vitro* and *in vivo* applications and has been proven to have no adverse

Figure 16. Confocal fluorescent microscope images of (a) cellular-type structure containing fluorescein microparticles; (b) precise spatial distribution of biodegradable microparticles within photopolymerized scaffold structures; (c) three-dimensional reconstructed confocal image of a microfabricated scaffold structure with spatially patterned fluorescein and rhodamine encapsulated microparticles.

Table 3. Characteristics of fabrication techniques

Fabrication Techniques	Critical Dimension	Throughput	Solvent	Feature Flexibility	Tool Cost
μ-imprinting lithography	~50 nm	high	none	2-D structures	Master is expensive
Soft lithography	~50 nm	high	organic solvent	3-D is possible by laminating	Soft master is inexpensive
Direct deposition	~5 μm	low	organic solvent	Simple geometry	Tools are simple and inexpensive
Three-dimensional printing	~0 μm	low	organic solvent	Any 3-D structures	High resolution ink-jet system required
Laser stereolithography	~10 μm	low	water as solvent	Any 3-D structures	High resolution positioning system required
Laser micromachining	~1 μm	intermediate	none	2-D structures	high resolution positioning system required
Nanosphere lithography	~100 nm	high	none	Restricted by self-assembled sphere patterns	cheap

effect on cells for a sufficient period of time. It is not cell adhesive without cell adhesion proteins (i.e. arginine-glycine-aspartic acid). By spatially encapsulating cell adhesion proteins, we could control cell attachment and growth. Ten percent (wt/vol) resin has a viscosity close to that of water. Increasing the concentration leads to higher viscosity. The resin is stable under normal experimental conditions, although sunlight should be minimized since it carries UV light. The curing speed depends on the UV sensitivity of the resin. High sensitivity indicates that a fast processing speed could be achieved. In our experiment, the pulse laser with 9 Hz repetition rate scanned the resin at a speed of 50 μm/sec. Typically, one laser pulse was enough to induce the curing. The resin can be cured only at the laser focal point; the uncured resin is reasonably stable under scattered or reflected UV light. With the PEGDMA resin and the 355-nm laser, a maximum resolution of 20 μm could be obtained. Though the resulting scaffold is relatively soft and fragile in an aqueous environment, it has good tensile strength when water is extracted.

6. SUMMARY AND FUTURE PROSPECTS

We summarize the important characteristics of each fabrication technique in Table 3. By employing newly developed fabrication techniques, with manufacturing costs and biocompatibility in mind, we can engineer a micro- or nano-scale biomimetic environment. These approaches allow us to study molecular interactions at the cellular level and to control drug delivery. Top-down approaches, some of which are reviewed in this chapter, provide great flexibility and control of the structures on a micron or submicron scale. Bottom-up approaches, which involve molecular-scale self-assembly, are widely believed to have great potential in terms of fabricating nanoscale devices. We anticipate that the combination of top-down and bottom-up approaches will lead to new technologies in the fabrication of biodegradable polymeric micro- and nanodevices for biomedical applications.

ACKNOWLEDGEMENTS

This work was supported by a CAREER award (DMI 0222014) to SC from the U.S. National Science Foundation. The SEM analysis was conducted in the Texas Materials Institute at the University of Texas at Austin. The authors acknowledge J. Mendenhall (ICMB Core Microscopy Facility, University of Texas at Austin) for his support on laser scanning confocal microscopy.

REFERENCES

1. J. T. Santini, A. C. Richards, R. Scheidt, M. J. Cima, and R. Langer, *Angew. Chem. Int. Ed. Engl.* 39, 2396 (2000).
2. T. A. Desai, W. H. Chu, J. K. Tu, G. M. Beattie, A. Hayek, and M. Ferrari, *Biotechnol. Bioeng.* 57, 118 (1998).
3. A. Ahmed, C. Bonner, and T. A. Desai, *J. Control. Release* 81, 291 (2002).
4. M. L. Reed, C. Wu, J. Kneller, S. Watkins, D. A. Vorp, A. Nadeem, L. E.Weiss, K. Rebello, M. Mescher, A. J. C. Smith, W. Rosenblum, and M. D. Feldman, *J. Pharm. Sci.* 87, 1387 (1998).
5. J. Wilbur, A. Kuman, H. Biebuyck, E. Kim, and G. M. Whitesides, *Nanotechnology* 7, 452 (1996).
6. M. S. Widmer, P. K. Gupta, L. Lu, R. K. Meszlenyi, G. R. D. Evans, K. Brandt, T. Savel, A. Gurlek, C. W. Patrick, Jr., and A. Mikos, *Biomaterials* 19, 1945 (1998)
7. A. G. Mikos, Y. Bao, L. G. Cima, D. E. Ingber, J. P. Vacanti, and R. Langer, *J. Biomed. Mater. Res.* 27, 183 (1993).
8. A. G. Mikos, G. Sarakinos, S. M. Leite, J. P. Vacanti, and R. Langer, *Biomaterials* 14, 323 (1993).
9. R. Langer, *Science* 249, 1527 (1990).
10. E. Holy, J. A. Fialkov, J. E. Davies, and M. S. Shoichet, *J. Biomed. Mater. Res. Part A* 15, 447 (2003).
11. P. X. Ma and R. Zhang, *J. Biomed. Mater. Res.* 15, 469 (2001).
12. D. H. Lewis, in "Biodegradable Polymers as Drug Delivery Systems" (M. Chasin and R. Langer, Eds.), Vol. 45, pp. 1–8. Marcel Dekker, New York, 1990.
13. C. Miller, H. Shanks, A. Witt, G. Rutkowski, and S. Mallapragada, *Biomaterials* 22, 1263 (2001).
14. D. K. Armani and C. Liu, *J. Micromech. Microeng.* 10, 80 (2000).
15. C. G. Pitt, , in "Biodegradable Polymers as Drug Delivery Systems" (M. Chasin and R. Langer, Eds.), Vol. 45, pp. 71–119. Marcel Dekker, New York, 1990.
16. W. W. Duley, "Laser Processing and Analysis of Materials." Plenum Press, New York, 1983.
17. D. Bäuerle, in "Laser Processing and Chemistry," pp. 259–281. Springer, New York, 2000.
18. A. Vogel, P. Schweiger, A. Friieser, M. N. Asiyo, and R. Birngber, *IEEE J. Quant. Elect.* 26, 2240 (1990).
19. E. W. Williams, "The CD-ROM and Optical Recording Systems," Oxford University Press, Oxford, 1994.
20. S. C. Chen, C. P. Griporopoulos, H. K. Park, P. Kersterns, and A. C. Tam, *J. Appl. Phys.* 85, 5618 (1999).
21. M. M. Ivanenko, T. Mitra, and P. Hering, *SPIE Proc. Optical Biopsy and Tissue Optics* 4161 (2000).
22. X. Liu, D. Du, and G. Mourou, *IEEE J. Quant. Elect.* 33, 1706 (1997).
23. S. C. Chen, D. G. Cahill, and C. P. Grigoropoulos, *J. Heat Transfer* 122, 107 (2000).
24. R. C. Crafer and P. J. Oakley, "Laser Processing in Manufacturing," Chapman & Hall, New York, 1993, pp. 1–20.
25. V. S. Letokhov, "Nonlinear Laser Chemistry: Multiple-photon Excitation," Springer, New York, 1983.
26. V. Kancharla and S. C. Chen, *Biomed. Microdev.* 4, 105 (2002).
27. S. C. Chen, V. Kancharla, and Y. Lu, *Int. J. Mater. Prod. Technol.* 18, 457 (2003).
28. P. Laurens, M. Ould Bouali, F. Meducin, and B. Sadras, *Appl. Surf. Sci.* 154, 211 (2000).
29. D. Knittel and E. Schollmeyer, *Polym. Intern.* 45, 110 (1998).
30. M. A. Roberts, J. S. Rossier, P. Bercier, and H. Girault, *Anal. Chem.* 69, 2035 (1997).
31. S. L. R. Barker, D. Ross, M. J. Tarlov, M. Gaitan, and L. E. Locascio, *Anal. Chem.* 72, 5925 (2000).
32. E. Betzig and J. K. Trautman, *Science* 257, 189 (1992).
33. M. Ohtsu and H. Hori, "Near-field Nano-optics," pp. 1–10. Kluwer Academic, New York, 1999.
34. Y. F. Lu, Z. H. Mai, G. Qiu, and W. K. Chim, *Appl. Phys. Lett.* 75, 2359 (1999).
35. S. M. Huang, M. H. Hong, Y. F. Lu, B. S. Luk'yanchuk, W. D. Song, and T. C. Chong, *J. Appl. Phys.* 91, 3268 (2002).
36. J. A. DeAro, R. Gupta, A. J. Heeger, and S. K. Buratto, *Synth. Met.* 102, 865 (1999).
37. Y. Lu, S. Theppakuttai, and S. C. Chen, *Appl. Phys. Lett.* 82, 4143 (2003).
38. Y. Lu and S. C. Chen, *Nanotechnology* 14, 505 (2003).
39. S. Theppakuttai and S. C. Chen, *Appl. Phys. Lett.* 83, 758 (2003).
40. U. C. Fischer and H. P. Zingsheim, *J. Vac. Sci. Technol.* 19, 881 (1981).
41. N. Denkov, O. Velev, P. Kralchevski, I. Ivanov, H. Yoshimura, and K. Nagayama, *Langmuir* 8, 3183 (1992).
42. P. A. Kralchevsky and K. Nagayama, *Langmuir* 10, 23 (1994).
43. R. Micheletto, H. Fukuda, and M. Ohtsu, *Langmuir* 11, 3333 (1995).
44. O. Watanabe, T. Ikawa, M. Hasegawa, M. Tsuchimori, and Y. Kawata, *Appl. Phys. Lett.* 79, 1366 (2001).
45. S. Y. Chou, P. R. Krauss, and P. J. Renstrom, *Appl. Phys. Lett.* 67, 3114 (1995).
46. H. W. Lehmann, R. Widmer, M. Ebnoether, A. Wokaun, M. Meier, and S. K. Miller, *J. Vac. Sci. Technol. B* 1, 1207 (1983).
47. F. Gottschalch, T. Hoffmann, C. M. S. Torres, H. Schulzb, and H.-C. Scheer, *Solid-State Electronics* 43, 1079 (1999).
48. N. Patel, R. Padera, G. H. W. Sanders, S. M. Cannizzaro, M. C. Davies, R. Langer, C. J. Roberts, S. J. B. Tendler, P. M. Williams, and K. M. Shakessheff, *FASEB* 12, 1447 (1998).
49. C. S. Chen, M. Mrksich, S. Huang, G. M. Whitesides, and D. E. Ingber, *Science* 176, 1425 (1997).
50. Y. N. Xia and G. M. Whitesides, *Annu. Rev. Mater. Sci.* 28, 153 (1998).
51. R. Landers and R. Mühaupt, *Macromol. Mater. Eng.* 282, 17 (2000).
52. G. Vozzi, C. Flaim, A. Ahluwalia, and S. Bhatia, *Biomaterials* 24, 2533 (2003).
53. I. Zein, D. W. Hutmacher, K. C. Tan, and S. H. Teoh, *Biomaterials* 23, 1169 (2003).
54. N. K. Vail, J. W. Barlow, J. J. Beaman, H. L. Marcus, and D. L. Bourell, *J. Appl. Polym. Sci.* 9, 789 (1994).

55. B. M. Wu, S. W. Borland, R. A. Giordano, L. G. Cima, E. M. Sachs, and M. J. Cima, *J. Control. Release* 40, 77 (1996).
56. T. Hagiwara, *Macromol. Symp.* 175, 397 (2001).
57. M. N. Cooke, J. P. Fisher, D. Dean, C. Rimnac, and A. G. Mikos, *J. Biomed. Mater. Res. Part B: Appl Biomater.* 64B, 65 (2002).
58. T. Matsuda, M. Mizutani, and S. C. Arnold, *Macromolecules* 33, 795 (2000).
59. Y. Lu, G. Mapili, S. C. Chen, and K. Roy, "Proceedings of the 30th Annual Meeting and Exposition," Glasgow, Scotland, 2003.